

Models of garnet differential geochronology

Matthew J. Kohn *

Department of Geosciences, Boise State University, 1910 University Drive, MS1535, Boise, ID 83725-1535, USA

Received 26 February 2008; accepted in revised form 7 October 2008; available online 14 October 2008

Abstract

Rayleigh distillation models are developed to describe theoretical growth zoning of Lu, Hf, Rb, Sr, Sm, and Nd in typical garnet crystals from metapelites and metabasites. Effects of diffusion-limited transport within the matrix and intracrystalline diffusion are also considered qualitatively. Theoretical zoning profiles show strong depletions of Lu in garnet rims compared to cores, but virtually invariant Hf, Rb, Sr, Sm, and Nd profiles, generally consistent with natural profiles for Lu and Hf and previously published models. Theoretical isochron diagrams for Lu–Hf exhibit distinctive arcuate distributions and high MSWDs consistent both with Himalayan data, and with expectations that garnet growth durations exceed chronologic resolution by as much as an order of magnitude. Predicted isochron diagrams for Sm–Nd and Rb–Sr exhibit vertical arrays for garnet and high MSWDs that are generally lower than for Lu–Hf in metapelites. Inherent chronologic resolution for bulk separates is best for Lu–Hf in metapelites and Rb–Sr, but analytical considerations favor Rb–Sr or Sm–Nd for chronologic zoning studies. Diffusion-limited transport in the rock matrix strongly influences zoning profiles, but does not change the main trends on isochron diagrams. Intracrystalline diffusion will initially rotate Lu–Hf isochrons to steeper slopes, giving older apparent ages. The natural Himalayan data indicate growth of garnet in one rock from the Greater Himalayan Sequence at ~34 Ma, consistent with previously measured monazite ages from the same rock. Data from another Himalayan rock suggest polymetamorphism that includes a Paleozoic component.

© 2008 Elsevier Ltd. All rights reserved.

1. INTRODUCTION

The advent of high-precision Lu–Hf analysis by multi-collector ICP-MS and increased sensitivity of TIMS instrumentation for Sm–Nd and Rb–Sr analyses have led to unprecedented age resolution for garnet and a wealth of new data for petrologic and tectonic research. One putatively discouraging feature of some garnet isochrons is a high MSWD, which might traditionally be viewed as indicating “bad data” due to such factors as inclusions in the garnet or problems in analytical methods. Although several factors affect chronologic data, theoretical Rayleigh distillation models are developed here and compared to natural data to illustrate that the high chronologic resolution afforded by technical advances demands high MSWDs, at least if garnet growth occurs over Myr to tens of Myr. The pur-

pose of this paper is to develop the theoretical basis for these models, to present theoretical chemical and isotopic zoning profiles that might be used in interpreting *in situ* analyses, to show the effects of progressive garnet growth on isochron diagrams and on chronologic age disparities for different isotopic systems, and to compare results with natural data from garnet separates from Himalayan metapelites.

Rayleigh distillation models for Lu–Hf and Sm–Nd were already considered by Lapen et al. (2003), and Skora et al. (2006) modeled diffusion-limited REE uptake profiles in metabasites. However assumed partition coefficients for Lu (Lapen et al., 2003) and Sm (Skora et al., 2006) are far different than typical garnet–whole-rock fractionations. Distributions of data on isochron diagrams and the Rb–Sr system were well beyond the scope of both previous studies, as well as the influence of intracrystalline diffusion on isochrons, or the chronologic resolvability of different isotopic systems (either for *in situ* analysis of zoned crystals, or for bulk analysis of garnet crystals that may

* Fax: +1 208 426 4061.

E-mail address: mattkohn@boisestate.edu

have nucleated at different times). In light of increasing chronologic data for garnet through the advent of MC-ICP-MS analysis and advances in TIMS analysis of smaller aliquots, a more comprehensive study appears timely. The results presented here are not intended to supplant the seminal work of Lapen et al. (2003) and Skora et al. (2006), but rather to build upon them.

The first and largest component of this paper explores theoretical zoning profiles in garnet crystals and their implications for isotopic zoning and isochrons. Particular emphasis is placed on origins of data scatter and chronologic resolution of different isotopic systems. The second component presents natural data from two Himalayan rocks, illustrating some of the principal predictions of the theoretical models, both in terms of trace element zoning, and for isochron diagrams. In this discussion, the adjective “radiogenic” is used to describe the magnitude of the ratio between the daughter and reference isotopes (e.g., $^{176}\text{Hf}/^{177}\text{Hf}$): large vs. small values are more vs. less radiogenic. The term “MSWD” (Mean Square of Weighted Deviates) basically reflects the scatter of the data about the best-fit line compared to the scatter expected from analytical errors, and is equivalent to the RMSE (Root Mean Square Error).

2. METHODS AND SAMPLES

2.1. Garnet growth models

Quantitative models were based on Rayleigh distillation (Rayleigh, 1896), according to the expression (Hollister, 1966, 1969; Hoefs, 1997):

$$C_i^M = \alpha_i C_{i,o}^R f^{\alpha_i - 1} \quad (1)$$

where C_i^M is the concentration of the species i in the mineral, α_i is the partition coefficient (or fractionation factor, sometimes labeled λ) for species i in the mineral relative to the rock, $C_{i,o}^R$ is the initial concentration in the rock matrix, and f is the fraction of the species i remaining in the rock ($= 1 - \frac{W_{Grt}}{W_o}$, where W_{Grt} is the mass of garnet and W_o is the original mass of the rock). Table 1 summarizes input parameters used for modeling.

Partition coefficients for Lu–Hf in metapelites were estimated by comparing whole-rock compositions with garnet core compositions for allanite-free metapelites analyzed by Corrie and Kohn (2008) and have 2σ uncertainties of a factor of ~ 2 . These factors implicitly assume Hf contents for whole-rocks that include zircon.

Assuming a lower Hf content for the reactive component of a rock (i.e., assuming most zircon is unreactive) would increase the Hf partition coefficient, but would not significantly affect the modeled garnet Hf content or Lu/Hf ratio. Predicted core Lu/Hf ratios are >100 times higher than modeled by Lapen et al. (2003); (whose models are otherwise similar), and similar to Skora et al. (2006); (whose models are otherwise different). Partition coefficient differences compared to Lapen et al. (2003) lead to major differences in the magnitude and character of Lu and Lu/Hf zoning, and implications for garnet Lu–Hf isochrons. The Lu–Hf partition coefficients for metabasites were estimated from rocks analyzed by King et al. (2004, 2007), Corrie et al. (2007), and Cheng et al. (2008); the Lu partition coefficient is similar to that determined for allanite-bearing metapelites (Corrie and Kohn, 2008), and is lower than for allanite-free metapelites probably because matrix epidote-group minerals or titanite more strongly fractionate REE than in Ca-poor bulk compositions (e.g., see Hermann, 2002; Thöni, 2002).

Different chronologic and trace element studies have yielded inconsistent garnet-whole-rock partition coefficients for Sm–Nd. These discrepancies must result in part from variable contamination of garnet separates by inclusions (e.g., see Amato et al., 1999; Jung and Mezger, 2001, 2003a,b), and possibly also from differences in Sm partitioning depending on mineral assemblage (e.g., Hickmott, 1988; Hickmott and Spear, 1992; Hermann, 2002; Thöni, 2002), much as is observed for Lu in metapelites vs. metabasites. Values in Table 1 are based on chronologic studies of leached garnets (Amato et al., 1999; Jung and Mezger, 2001, 2003a,b; Baxter and DePaolo, 2002; Baxter et al., 2002; Anczkiewicz et al., 2007), adjusted for trace element studies demonstrating somewhat stronger partitioning of Sm/Nd (Hickmott et al., 1987; Hickmott and Spear, 1992). These values and resulting Sm/Nd ratios are similar to those used by Lapen et al. (2003) and at the upper end of values for metabasites and metapelites summarized by Thöni (2002), but 40 times lower than the value assumed by Skora et al. (2006).

Partition coefficients for Rb–Sr were taken from compositions measured by Christensen et al. (1989, 1994; see also Jung and Mezger, 2001). Whole-rock concentrations of Lu, Hf, Sm, Nd, Rb, and Sr were derived from diverse sources that include sedimentary rocks (Taylor and McLennan, 1985) and metamorphic rocks (Christensen et al., 1989, 1994; King et al., 2004; Corrie et al., 2007; Corrie and Kohn, 2008; Cheng et al., 2008). Results depend negligibly on assumed whole-rock concentrations and on all partition coefficients except for Lu.

In each model, garnet growth was modeled until it attained 5% of the rock by weight, over a period of 10 Myr. This duration was sufficient to generate interesting intracrystalline isotopic variations, and is well within the durations estimated from direct core-rim measurements of isotopic ratios in garnets analyzed by Rb–Sr and Sm–Nd (e.g., Christensen et al., 1989, 1994; Johnston et al., 2007), or through intercomparisons of different isotopic systems (Lapen et al., 2003; Kylander-Clark et al., 2007). Greater amounts of garnet could be readily modeled, but in general zoning patterns become more P–T path and bulk composition-dependent when metamorphism is more protracted and when different reactions or phase stability boundaries are encountered (e.g., Spear et al., 1990). Thus, trace element zoning in natural metamorphic garnets should always be measured to evaluate correspondence with idealized models (Lapen et al., 2003; Skora et al., 2006; Cheng et al., 2008; Schmidt et al., 2008; this study). Different growth models were considered, including linear growth of garnet with respect to crystal radius, area, or volume, with appropriate scaling in plots of composition vs. distance (Figs. 1–4). An exponential growth model was also constructed, assuming that the total amount of garnet at time t is equal to $[M_f(e^{5t} - 1)]/[e^{5t(f)} - 1]$, where M_f is the final amount of garnet (5 wt%), t is time, and $t(f)$ is the total duration of garnet

Table 1
Input parameters used for modeling.

Rock	Parent	α_{parent}	Mtx conc. (ppm)	Daughter	α_{Daughter}	Mtx conc. (ppm)
Pelite	^{176}Lu	100	1	^{176}Hf	0.040	5
Metabasite	^{176}Lu	25	0.2	^{176}Hf	0.050	3
Pelite	^{87}Rb	0.0035	200	^{87}Sr	0.040	200
Pelite	^{147}Sm	0.25	5	^{143}Nd	0.015	25

Note: All models assume growth of 5% garnet (by weight) over a period of 10 Myr. Exponential model uses same parameters as pelite, but garnet growth accelerates exponentially in 5 t. See text for partition coefficient data sources.

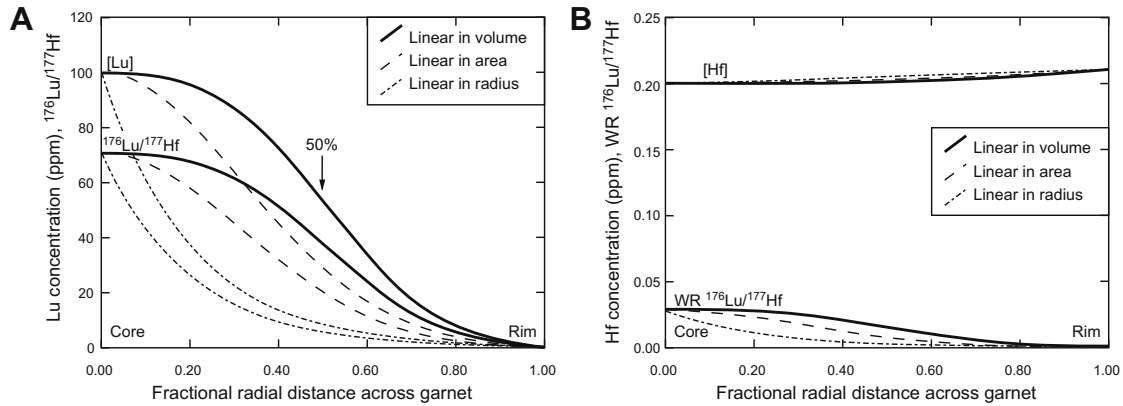


Fig. 1. Modeling results for Lu–Hf zoning for a metapelite garnet, assuming growth of garnet is linear in volume, area, or radius (i.e., constant dV/dt , dA/dt , and dr/dt). (A) Lu concentration and $^{176}\text{Lu}/^{177}\text{Hf}$ from core to rim. For model that is linear in volume, 50% of Lu in the garnet is coreward of the arrow. (B) Hf concentration from core to rim, and whole-rock $^{176}\text{Lu}/^{177}\text{Hf}$ during growth of garnet. Whole-rock composition (WR) refers to compositional evolution of garnet-free matrix.

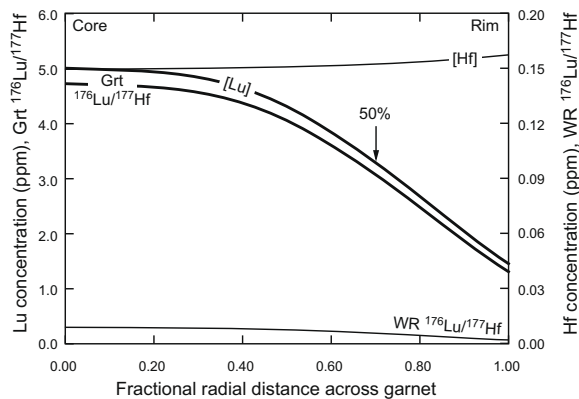


Fig. 2. Modeling results for Lu–Hf intracrystalline zoning for garnet from a metabasite, assuming linear growth with respect to volume, showing core-rim zoning in Lu and Hf concentrations and $^{176}\text{Lu}/^{177}\text{Hf}$, as well as whole-rock $^{176}\text{Lu}/^{177}\text{Hf}$ during growth of garnet. Fifty percent of Lu in the garnet is coreward of the arrow. Whole-rock composition (WR) refers to compositional evolution of garnet-free matrix.

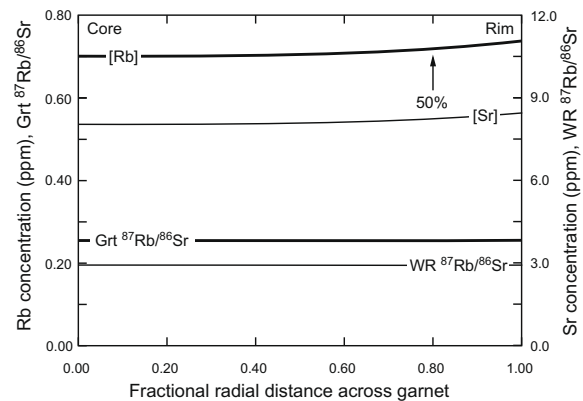


Fig. 3. Modeling results for Rb–Sr intracrystalline zoning for a metapelite garnet, assuming linear growth with respect to volume, showing core-rim zoning in Rb and Sr concentrations and $^{87}\text{Rb}/^{86}\text{Sr}$, as well as whole-rock $^{87}\text{Rb}/^{86}\text{Sr}$ during growth of garnet. Fifty percent of Rb in the garnet is coreward of the arrow. Whole-rock composition (WR) refers to compositional evolution of garnet-free matrix.

growth. This function was chosen simply to illustrate effects of variable garnet growth rates on predicted profiles. Theoretical results are plotted in terms of trace element concentration and isotope ratio vs. distance across model garnets from core to rim (Figs. 1–4), and shifts to isotope ratio relative to initial ratio vs. distance across model garnets from core to rim (Fig. 5). These plots show expected results for analyses collected by either microsampling or *in situ* line traverses.

The effects of diffusion-limited transport in the matrix were also considered qualitatively for all systems, assuming slow diffusion for Lu, Hf, Sm, Nd, and Sr. Rb was considered either as similarly slow-diffusing, or as fast-diffusing. Models of REE uptake were already considered more quantitatively and completely by Skora et al. (2006), and results are generalized and extrapolated here for chronologic systems. Diffusional modification of growth zoning was also considered. Broad chemical trends in the matrix and garnet crystals were inferred based on major and trace element zoning observed in natural samples (e.g., Kohn, 2003).

2.2. Sampling and sample processing strategies

Sampling strategies affect both the analytical resolution of isotopic measurements, which affects data plotting and calculation of MSWDs, and the spatial resolution of an analysis within a garnet. Traditionally, garnets are separated from powdered rock, with different splits reflecting different physical characteristics; the correspondence between each split and the compositional domain(s) within the garnet is not known *a priori*. Commonly it is assumed that garnet in a rock has “an” age, and that different splits either sample portions of the garnet with different parent–daughter ratios, or are variably contaminated with cosanguineous inclusions. Physical separation of different garnet splits, sometimes combined with differential leaching to remove inclusions (e.g., Zhou and Hensen, 1995; DeWolf et al., 1996; Amato et al., 1999; Anczkiewicz and Thirlwall, 2003), causes dispersion on isochron diagrams and improves age confidence. In reality, different garnet generations or portions of a garnet may differ in size, color (chemistry), magnetic properties or inclusion density, if cores have more inclusions than

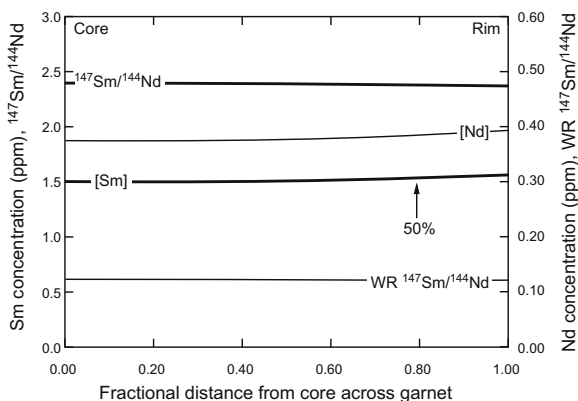


Fig. 4. Modeling results for Sm–Nd intracrystalline zoning for a metapelitic garnet, assuming linear growth with respect to volume, showing core-rim zoning in Sm and Nd concentrations and ¹⁴⁷Sm/¹⁴³Nd, as well as whole-rock ¹⁴⁷Sm/¹⁴³Nd during growth of garnet. Fifty percent of Sm in the garnet is coreward of the arrow. Whole-rock composition (WR) refers to compositional evolution of garnet-free matrix.

rims (or vice versa), so distinguishing splits based on physical criteria may partially separate cores from rims. These effects would not only cause dispersion on isochron diagrams, assuming garnets are zoned in parent–daughter ratios, but also imply potentially resolvable age differences and high MSWDs, if garnet growth was protracted. These factors are considered in constructing the model isochrons. Such bulk samples (hundreds of mg) provide non-limiting amounts of isotopes for measurement, so relatively small uncertainties of ±0.000015 for Hf isotopes (~0.005%), ±0.000007 for Sr isotopes (~0.001%) and ±0.000005 for Nd isotopes (~0.001%) are assumed.

Alternatively, garnets may be microsampled for Sr or Nd isotope measurement (e.g., Christensen et al., 1989; Ducea et al., 2003). The intention of this approach is to identify core-rim differences in isotopic compositions and ages, and application of isochrons to different garnet analyses is rarely warranted because

one assumes *a priori* that ages may be significantly different. This type of analysis is, however, discussed in terms of age resolution and in comparison to predicted isotopic profiles. Because Hf-isotopic analysis currently requires such large samples, only Rb–Sr and Sm–Nd systems are considered for microsampling, with moderately increased analytical uncertainties because of reduced sample sizes.

Sample leaching is commonly applied to remove contaminating inclusions, which can be the bane of Sm–Nd dating (Zhou and Hensen, 1995; DeWolf et al., 1996; Amato et al., 1999; Anczkiewicz and Thirlwall, 2003). The Lu–Hf dating method is much less sensitive to inclusions because garnet Lu concentrations are high, and because contamination by Hf-rich phases can be readily avoided. Few common minerals except zircon and rutile take up significant Hf, and benchtop dissolution minimizes any zircon and rutile contamination (e.g., Scherer et al., 2000; Connelly, 2006; Lagos et al., 2007). For example, high Lu/Hf ratios (≥100) are expected from *in situ* measurements that show typical Lu concentrations in garnet cores of several tens of ppm to >100 ppm, but Hf concentrations consistently ≤~0.5 ppm (e.g., Hermann, 2002; Skora et al., 2006; Corrie and Kohn, 2008; this study). These data imply ¹⁷⁶Lu/¹⁷⁷Hf ratios ≥10, at least for garnet cores. This fact is well illustrated in a study of Greek eclogites (Lagos et al., 2007), where benchtop dissolutions yielded Lu and Hf concentrations of several tens of ppm and ≤0.5 ppm respectively (¹⁷⁶Lu/¹⁷⁷Hf ratios up to ~50), completely consistent with *in situ* studies. In contrast, bomb dissolutions of these same separates yielded similar Lu concentrations, but Hf concentrations up to several ppm (¹⁷⁶Lu/¹⁷⁷Hf ratios ≤~1), indicating major contamination by extraneous Hf. Similarly, concentrations of Hf in Himalayan garnets described in this study are all ≤~0.25 ppm, indicating minimal dissolution of zircon and rutile, and Lu concentrations range up to ~50 ppm (¹⁷⁶Lu/¹⁷⁷Hf ratios up to ~14).

2.3. Model Isochrons

Model isochrons (Fig. 6) were constructed assuming bulk separate analyses, where different generations of garnet nucleated and grew at different points in each modeled rock’s history. The oldest generation of garnet was assumed to nucleate at 10 Ma (the start of

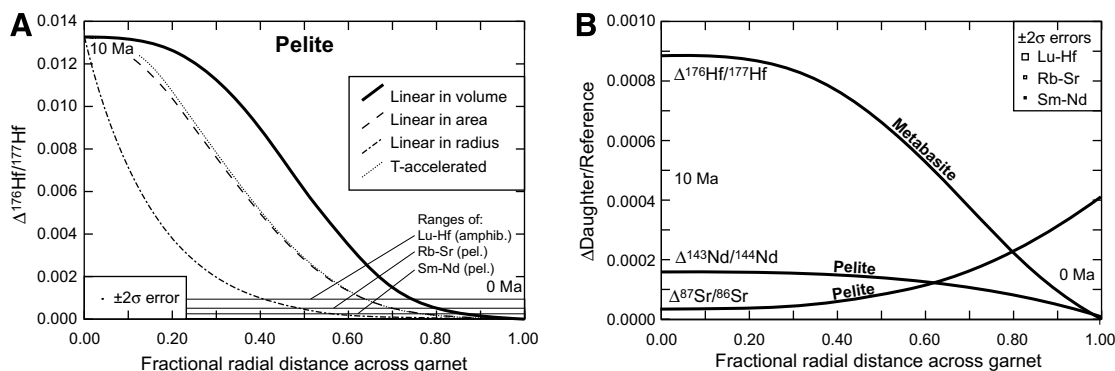


Fig. 5. Modeling results for intracrystalline zoning in the change in ratio of daughter isotope to reference isotope, relative to initial isotopic composition, assuming growth interval of 10 Myr. (A) Lu–Hf system for a metapelitic garnet with different growth models. “T-accelerated” = growth that is linear in volume (same chemical zoning pattern as in Fig. 1), but exponentially increases with increasing temperature (e.g., Carlson, 1989). Note large shifts to ¹⁷⁶Hf/¹⁷⁷Hf compared to typical ±2σ analytical errors, and inability of this system to distinguish some different growth models (e.g., linear in area vs. temperature-accelerated growth). (B) Lu–Hf system for garnet from a metabasite, and Sm–Nd and Rb–Sr systems for metapelitic garnet crystals. Shifts are smaller, but still readily measured for Lu–Hf and Rb–Sr. Distinguishing zoning analytically is most difficult for Sm–Nd system both because of relatively low parent–daughter ratio and much longer half-life for ¹⁴⁷Sm decay. Thin line in A bounds scale in B, emphasizing extreme isotopic torque of Lu–Hf system in metapelites. Note that curves for Lu–Hf and Sm–Nd do not quite intersect zero because of radioactive decay of whole-rock.

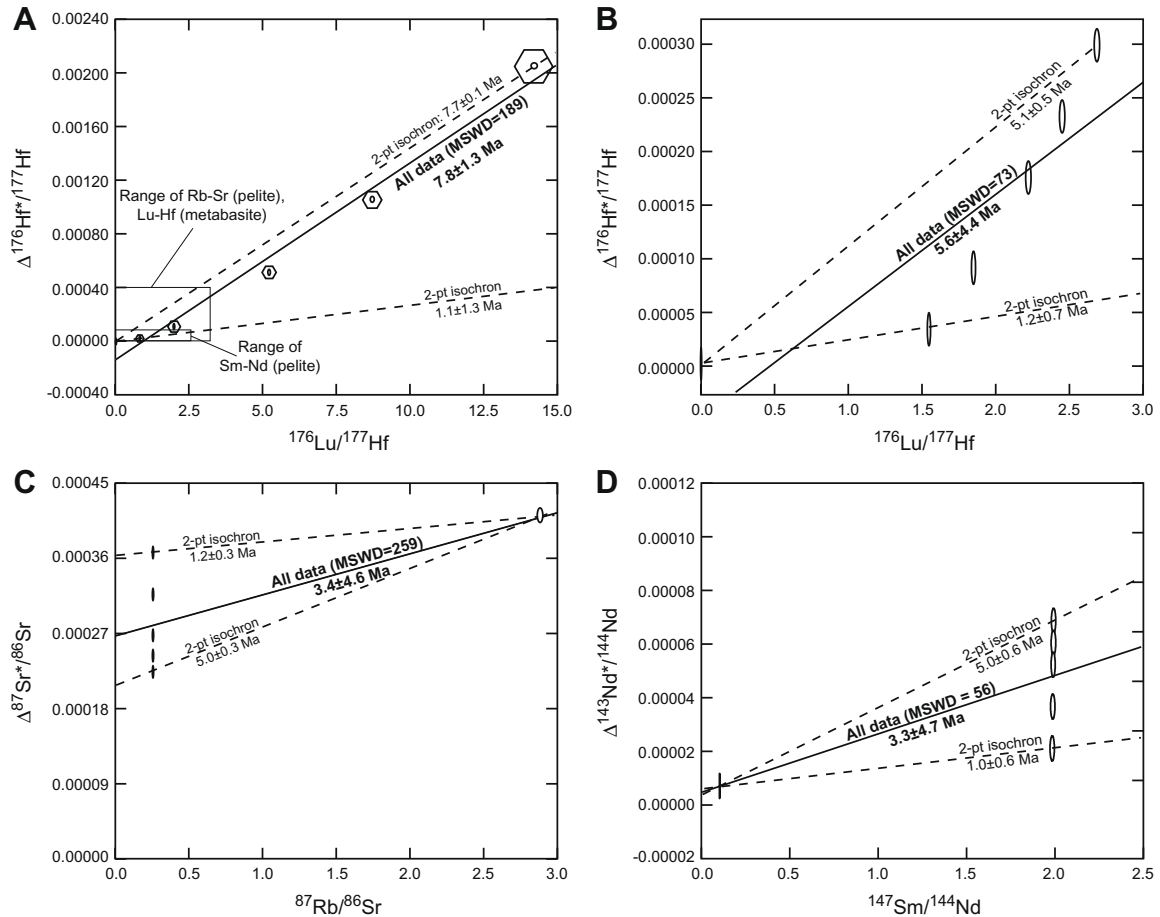


Fig. 6. Isochron diagram showing possible distributions of data for garnet crystals that nucleated at different times in a single model rock. Note arcuate distributions, particularly for Lu–Hf, with decreasing MSWD from A to D, reflecting decreasing ability of different isotopic systems to resolve duration of garnet growth. (A) Lu–Hf isochrons for metapelite, showing strong decrease in Lu/Hf for later-grown garnet crystals. Hexagons show relative sizes of different generation garnet crystals (assuming linear increase in volume with time). (B) Lu–Hf isochrons for metabasite. (C) Rb–Sr isochrons for metapelite. (D) Sm–Nd isochrons for metapelite. Data plotted and regressed using IsoPlot (Ludwig, 2001).

the model), and grow continuously until the present, at which time the bulk garnet would be separated and analyzed. Other garnet fractions correspond to nucleation at 8.75 Ma, 7.5 Ma, 5.0 Ma, and 2.5 Ma, with growth to the present. Plots (Fig. 6) assume that these different generations of garnet are somehow physically distinguishable. This distinction could be based on size, but any other criteria leading to similar preferential sampling of different garnet generations will lead to similar results. These results are not significantly different if compositions are selected from model zoning profiles (e.g., mimicking *in situ* analyses), although *in situ* analysis would provide greater ranges in isotopic values. Uncertainties in isotopic ratios were assumed to be 0.5% for interelement ratios. Data were regressed using IsoPlot (Ludwig, 2001).

2.4. Himalayan samples

The two samples analyzed in this study, 31a and 72b, were both collected as part of a regional metamorphic, chronologic, and tectonic analysis of Greater Himalayan rocks in the hanging wall of the Main Central Thrust, Langtang Valley, Nepal (Kohn et al., 2004, 2005; Kohn, 2008). Both derive from a basal unit, structurally ~1 km above the Main Central Thrust. The structurally lower sample, 31a, was collected close to a subunit boundary that was inferred based on the occurrence in garnet crystals of obvious

oscillatory zoning in Ca (Kohn, 2004). Calcium zoning in one grain from 31a could be construed as oscillatory (see [Electronic Annex](#)). Thus, differences in metamorphic history and chronology between 31a and 72b are possible. Major silicates include garnet + biotite + muscovite + plagioclase + quartz; sample 31a additionally contains kyanite. Rutile is common in sample 31a, and does occur as inclusions in garnet crystals. Garnet grain cores in sample 72b have abundant inclusions of quartz and ilmenite; rims are virtually inclusion-free. Some garnet grains in sample 31a show this general texture, but others have more uniformly distributed inclusions, and the core of one garnet crystal may be outlined by a ring of quartz inclusions ([Electronic Annex](#)). Peak P–T conditions were estimated at 750 °C and 10–12 kbar (Kohn, 2008).

X-ray maps ([Electronic Annex](#)) generally show core-rim concentric decreases in Mn (31a only) and Mg (both samples) typical of prograde metamorphism. The upturn in Mn and downturn in Mg at the rim clearly demonstrate intracrystalline modification of growth profiles. Note that sample 72b has unusually low Mn, but Mn maps of garnet grains from samples structurally above and below it show the same basic pattern as in sample 31a. Calcium maps show patchy zoning, typical of garnet crystals from these structural levels (Kohn et al., 2004). Except for a narrow low-Ca rim on the edges of garnet crystals from sample 31a, little in these maps suggests either a complex metamorphic history or mass

transport limitations within the matrix (e.g., Chernoff and Carlson, 1999; Skora et al., 2006).

2.5. Trace element analyses

Data were collected using laser-ablation ICP-MS at the Geo-analytical Laboratory, Washington State University. Samples were ablated along traverses using a NewWave frequency quintupled Nd-YAG laser ($\lambda = 213$ nm), operating at ~ 10 J/cm² and 10 Hz, with a 8–12 μ m diameter spot and stage motion rate of 5 μ m/s. Ablated material was carried on a He stream to the plasma source of a ThermoFinnigan Element2 (single collector, magnetic sector mass spectrometer). Analyses were collected in low-resolution mode ($m/\Delta m = 300$), using analog mode for ²⁷Al, and pulse counting for all other isotopes (⁴³Ca, ⁴⁵Sc, ⁴⁷Ti, ⁵⁵Mn, ⁵⁷Fe, ⁸⁹Y, ⁹⁰Zr, ¹⁵⁷Gd, ¹⁶³Dy, ¹⁶⁶Er, ¹⁷²Yb, ¹⁷⁵Lu and ¹⁷⁸Hf). Results for only Y, Lu, and Hf are presented here. Data were screened to remove analyses biased by inclusions. For quartz and ilmenite inclusions, the entire analysis was removed. Zircon inclusions do not significantly bias concentrations of Y, Lu or major elements, but strongly influence apparent Hf concentrations. Thus, for analyses with obvious zircon contamination Y and Lu were plotted, but Hf was not. Detection limits were $\leq \sim 0.25$ ppm, and a complete sweep through all isotopes of interest required 2 s, yielding an effective spatial resolution of 10 μ m. Analyses were standardized against NIST 612 glass, using ²⁷Al as an internal standard. Locations of plotted traverses are shown in Electronic Annex.

2.6. Lu–Hf analysis

Samples were crushed, split for whole-rock analyses, sieved, and hand-picked under a binocular microscope for different size garnet fractions ranging from >2 mm to 0.5–1.0 mm. For the largest size fraction (G3), whole garnet crystals were analyzed, so cores must have been analyzed, as well as abundant inclusions. Intermediate size fractions (G2) were identifiable fragments of larger crystals, many of which appeared to transect the core, but the relative proportion of core material in G2 vs. G3 cannot be estimated *a priori*. The smallest size fractions (G1) were picked focusing on minimizing visible inclusions, so must have preferentially sampled the garnet rims in 72b and possibly also in 31a.

Analyzed samples weighed 250–300 mg and were processed for Lu–Hf isotopic ratios at Washington State University based on established methods (Vervoort and Blichert-Toft, 1999; Vervoort et al., 2004). Excepting minor differences in sample dissolution, the complete method is described in detail by Cheng et al. (2008). To summarize dissolution procedures, garnets were weighed into Savillex[®] vials, leached in 1 M HCl in a room-temperature ultrasonic bath for ~ 5 min (whole-rocks were not), then rinsed twice in distilled water. The leach solution was clear and colorless in all cases except for the largest garnets from sample 72b. Split G3 garnets have minor red staining along through going fractures, and the first leach solution was slightly colored. Two more leaches at the same conditions yielded a colorless leach solution. All samples were wetted with a 1:10 HNO₃–HF mixture, dried overnight on a hotplate, then dissolved for 24–48 hours in a 1:9 HNO₃–HF mixture in sealed vials on a hotplate. Samples were dried, and fluorides were converted to soluble chlorides using a 1:2 orthoboric-hydrochloric acid mixture in sealed vials on a hotplate. Solutions after this step were clear, although commonly a fine residue of undissolved graphite, zircon, and rutile remained. Samples were dried overnight, taken up in HCl, spiked using a ¹⁷⁶Lu–¹⁸⁰Hf tracer, equilibrated for 1–2 days in sealed vials on a hotplate, then dried. Samples were taken up again in HCl-trace HF for column chemistry, which was based on the approach of Münker et al. (2001) and followed exactly the methods of Cheng et al. (2008). Lu/Hf ratios

and Hf-isotope analyses were collected with a Neptune multi-collector ICP-MS housed in the Geoanalytical Laboratory, Washington State University. Note that sample-spike equilibration using this method has been previously demonstrated (Vervoort et al., 2004). Unless in-run errors were larger, analytical precisions for ¹⁷⁶Hf/¹⁷⁷Hf and ¹⁷⁶Lu/¹⁷⁷Hf were assumed to be 0.000014 and 0.5% (2σ), respectively, based on external precisions on standard solutions and duplicates of rock standards (Vervoort et al., 2004).

3. RESULTS

3.1. Theoretical models

Theoretical models of garnet growth zoning (Figs. 1–4) show strong depletions of Lu from core to rim in garnet crystals from both metapelites and metabasites, although zoning is strongest in metapelitic garnets because the partition coefficient is much larger than for metabasites. Predicted zoning is weak for Hf, Sm, Nd, Rb, and Sr because all elements are strongly excluded from garnet relative to the matrix ($\alpha \ll 1$; see also Lapen et al., 2003; Skora et al., 2006). This exclusion progressively enriches these elements in the matrix, and causes slight increases from core to rim in the modeled garnet crystals. In the case of Lu–Hf, these trends mean that Lu/Hf strongly decreases from core to rim, as the matrix is stripped of Lu but remains a significant Hf reservoir (Figs. 1 and 2). For Rb–Sr and Sm–Nd, the matrix always remains the main reservoir, and concentrations and their ratios change little from core to rim (Figs. 3 and 4). Different garnet growth models produce different rates of decrease of Lu from core to rim (Fig. 1A), but minimal changes to Hf concentrations (Fig. 1B). Although not shown, Sm, Nd, Rb, and Sr concentrations also change little from core to rim for different garnet growth models.

Growth of garnet over 10 Myr causes large to moderate changes to ¹⁷⁶Hf/¹⁷⁷Hf (depending on bulk compositions), moderate changes to ⁸⁷Sr/⁸⁶Sr, and small changes to ¹⁴³Nd/¹⁴⁴Nd, expressed as $\Delta^{176}\text{Hf}/^{177}\text{Hf}$, etc. (Fig. 5). The magnitude of the shifts reflects the ratio of parent isotope (¹⁷⁶Lu, ⁸⁷Rb, ¹⁴⁷Sm) to reference isotope (¹⁷⁷Hf, ⁸⁶Sr, ¹⁴³Nd; Fig. 1–4), and the decay constant (fastest for ¹⁷⁶Lu, slowest for ¹⁴⁷Sm). With the highest parent-reference ratio and fastest decay rate, $\Delta^{176}\text{Hf}/^{177}\text{Hf}$ is highest for pelitic garnet crystals, whereas with a low Sm/Nd and slow decay rate, $\Delta^{143}\text{Nd}/^{144}\text{Nd}$ is smallest. Note that $\Delta^{176}\text{Hf}/^{177}\text{Hf}$ and $\Delta^{143}\text{Nd}/^{144}\text{Nd}$ are driven principally by the composition of the garnet itself, which has high parent-reference ratios and experiences considerable radiogenic isotope ingrowth. In contrast, in the Rb–Sr system it is the matrix that has high Rb/Sr, and $\Delta^{87}\text{Sr}/^{86}\text{Sr}$ in the garnet passively records matrix ingrowth (Christensen et al., 1989).

Standard isochron diagrams (Fig. 6) show arcuate distributions for Lu–Hf that result naturally from more radiogenic compositions with high parent-reference isotope ratios in the largest and earliest nucleated crystals, and progressively less radiogenic compositions with low parent-reference isotope ratios in the smallest and latest nucleated crystals. Progressive depletion of the matrix in Lu causes the later-grown garnet crystals to more closely approach the original matrix Lu/Hf. Strong Lu fractionation also results in an older 2-point isochron for the matrix plus oldest

garnet fraction compared to other isotopic systems, because more parent isotope is sequestered in garnet cores in this system than in the others. Less fractionation for metabasites, and for Rb–Sr and Sm–Nd, means that the parent-reference ratios change less, so the oldest 2-point isochrons more closely approximate average ages. In all cases, changes to matrix parent-reference isotope ratios are so small that use of whole-rock vs. garnet-free matrix compositions would insignificantly affect any chronologic interpretation. Pairing the most radiogenic garnet split with the matrix yields a minimum age for the nucleation of garnet (i.e., nucleation must be older), whereas pairing the least radiogenic split with the matrix yields a maximum age for the termination of garnet growth (i.e., the last garnet grown must be younger).

Modeled MSWD is greatest for Lu–Hf in the metapelite and for Rb–Sr (Fig. 6A, MSWDs of 189, 259), compared to Lu–Hf in the metabasite and Sm–Nd (Fig. 6B–D; MSWDs of 73, 56) meaning that the isotopic compositions in Fig. 6A and C are more separated, i.e., chronologically distinguishable, than in the other modeled systems. The slight overlap of the error ellipses for Sm–Nd (Fig. 6D) also indicates somewhat poorer discrimination of ages. The fact that 2-point isochrons have uncertainties approaching a few hundred kyr in all systems, whereas garnet growth is modeled as having occurred over millions of years necessitates high MSWDs if all porphyroblast data are regressed together to derive an average age.

Strong partition coefficients for Lu–Hf can lead to negative initial ϵ_{Hf} (compared to initial Hf isotopic compositions). Specifically, both Model 1 and Model 3 regressions of IsoPlot (McIntyre et al., 1966; York, 1966; Ludwig, 2001) yield negative initial ϵ_{Hf} for these synthetic data because the slope is controlled by the most radiogenic composition plus the matrix, whereas the less radiogenic splits pull the regressed line and intercept downward.

Strong fractionation of Lu, but not Sr or Sm in garnet grains relative to the matrix also implies that 2-point isochrons between bulk garnet and matrix will be oldest for Lu–Hf, and youngest for Sm–Nd and Rb–Sr (e.g., Lapen et al., 2003; Fig. 6A vs. Fig. 6C and D). These differences are generally small, however, typically no more than 30% of the growth duration (3 Myr for these models, Fig. 7). Small amounts of garnet growth yield more similar ages because there is little core-rim zoning. A maximum in age disparity occurs when garnet is 10–20% of the rock by weight (Fig. 7) because, for larger amounts of garnet growth, an increasingly significant amount of Lu is hosted in the outer rim, despite low Lu concentrations.

3.2. Effects of diffusion

Slow diffusion in the matrix causes more rapid depletion of Lu concentrations around a growing garnet, so the drop-off in Lu concentrations between core and rim is steeper than for fast diffusion in the matrix (Fig. 8A; Skora et al., 2006). For a constant rate of garnet growth, Lu concentrations at the boundary between garnet and matrix should eventually stabilize when depletion of the local matrix Lu from garnet growth is balanced by diffusional replenish-

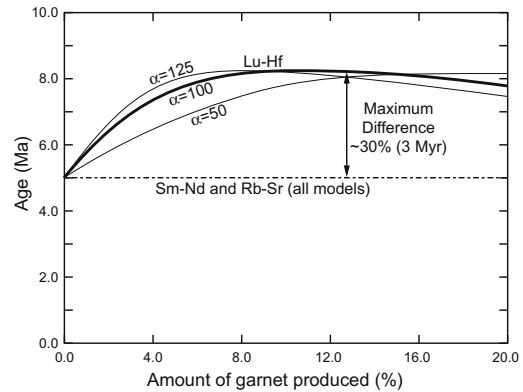


Fig. 7. Bulk garnet ages for Lu–Hf, Rb–Sr, and Sm–Nd for different amounts of garnet (wt% of garnet produced) and different possible partition coefficients for Lu. Ages for Lu–Hf show maximum ages for 10–20% garnet growth; Sm–Nd and Rb–Sr ages are essentially independent of the amount of garnet produced or the assumed partition coefficients. The maximum age difference between systems is likely to be only 30% of the total growth duration (i.e., ~3 Myr out of 10).

ment sourced by areas far removed from the garnet-matrix interface. The absolute Lu concentration depends on the balance between the rates of garnet growth vs. diffusion in the matrix. An additional complication will occur if later-grown garnet crystals nucleate in relatively Lu-rich matrix domains. Younger garnet cores will form with high Lu/Hf (unlike the simple Rayleigh distillation models, in which younger garnet crystals are increasingly depleted), but record much younger ages, leading to vertical distributions on isochron diagrams, similar to that predicted for Sm–Nd. A fully articulated model of diffusion-limited garnet growth would need to couple the diffusion rates of Lu and whatever element limits garnet growth with an increasing likelihood that garnet will nucleate in Lu-enriched domains.

In contrast to Lu, which is highly depleted around the growing garnet crystal, all other elements of interest, except perhaps Rb, are expected to “pile-up” at the crystal boundary, and their concentrations in the garnet should gradually increase as it grows (Fig. 8B–D; see Skora et al. for modeled profiles). If Rb diffuses as slowly as Sr, then the buildup of concentrations occurs at similar rates, and although Rb and Sr concentrations both increase in the garnet, their relative ratio remains virtually constant (Fig. 8B). A similar argument applies for Sm–Nd (Fig. 8D). If, however, Rb diffuses quickly compared to Sr, then the Rb/Sr ratio of the garnet gradually drops from core to rim (Fig. 8C).

With increasing temperature, intracrystalline diffusion in the garnet must eventually deplete the core in Lu via transport towards the garnet rim, and, if the garnet is dissolved, will enrich the rim in Lu (Fig. 9A). Hafnium concentrations are not expected to change significantly for two reasons. Firstly, Hf^{4+} diffuses about 2 orders of magnitude more slowly than REE^{3+} cations in zircon (Cherniak and Watson, 2003, 2007). Secondly Hf concentrations are so low and uniform there is little compositional gradient to drive diffusion. This latter consideration also applies to the elements Rb, Sr, Sm, and Nd, and although diffusion can cer-

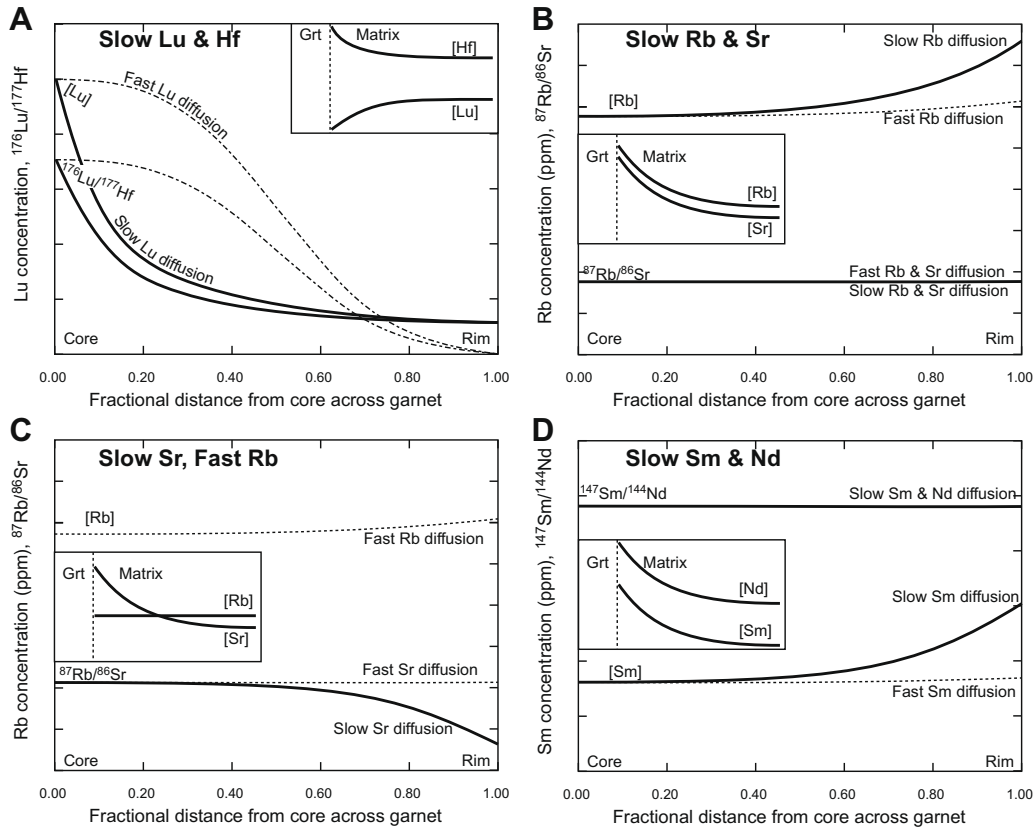


Fig. 8. Schematic diagrams showing effect of slow intercrystalline diffusion of parent and daughter isotopes on profiles of isotope concentrations and ratios in garnet and in matrix (insets). Dashed lines show models of fast diffusion in matrix (Figs. 1–4). (A) Lu–Hf assuming slow diffusion for both elements. (B) Rb–Sr assuming slow diffusion for both elements. (C) Rb–Sr assuming slow diffusion for Sr, but fast diffusion for Rb. (D) Sm–Nd assuming slow diffusion for both elements.

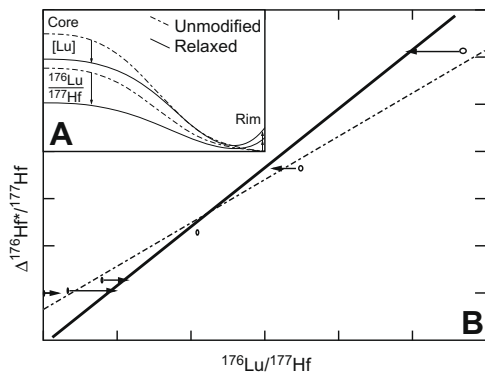


Fig. 9. Schematic diagrams illustrating effects of garnet dissolution and intracrystalline diffusion for Lu–Hf system in metapelites. The same types of effects will occur in other systems, but smaller compositional and isotopic gradients will diminish their magnitude. Dot-dash lines are unmodified compositions, solid lines are modified by diffusion. (A) Core–rim profiles of Lu concentration and Lu–Hf–isotope ratios in garnet, assuming faster intracrystalline diffusion of Lu^{3+} compared to Hf^{4+} . Concentrations of Lu decrease in garnet cores, and increase on rims. Matrix Lu concentrations also increase because of garnet dissolution. (B) Lu–Hf isochron, showing rotation to steeper slope (older apparent age) and decreased initial ϵ_{Hf} .

tainly control their closure in high-temperature systems (e.g., Burton et al., 1995), unlike Lu they are not expected to exhibit major changes in concentrations. If diffusion of Lu occurs after significant ingrowth of ^{176}Hf , then data will rotate anticlockwise on isochron diagrams (Fig. 9B), because cores and rims evolve to lower and higher parent-reference isotope ratios respectively. That is, intracrystalline diffusion initially increases apparent ages, and decreases inferred initial ratios.

3.3. Trace element zoning

Trace element zoning across Himalayan metapelitic garnet crystals (Fig. 10A and B) shows general trends consistent with the models of metapelites, including strong depletions in Lu (and Y) from core to rim. Hafnium concentrations can be heavily biased by microinclusions of zircon, but in regions where apparent Zr concentrations are low, mean Hf concentrations are <0.1 ppm, confirming the strong elemental fractionations implied by the Lu–Hf models. Both samples show near-rim increases in Lu and Y, interpreted to result from retrograde net-transfer reactions (ReNTRs) during cooling (Kohn and Spear, 2000), with significant back-diffusion towards the garnet interior, even for Y and HREE. These data imply that temperatures

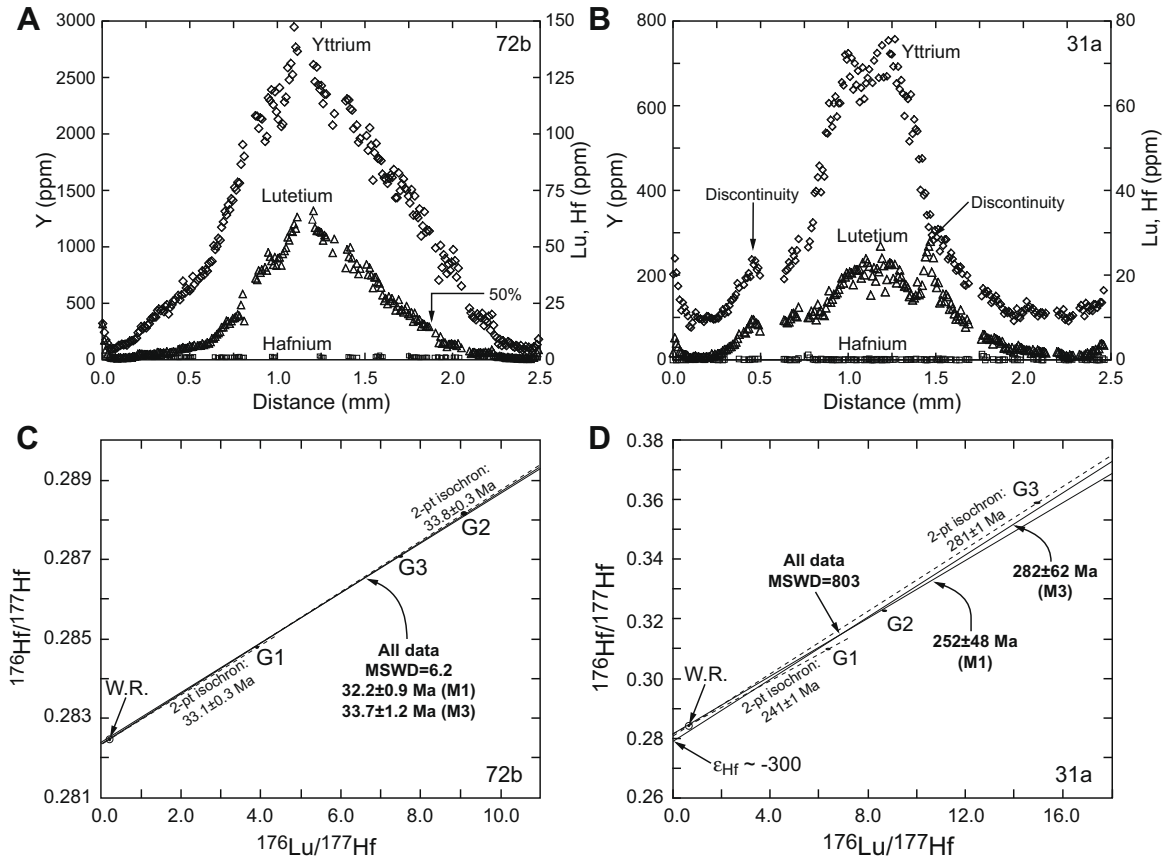


Fig. 10. Data from 2 Himalayan metapelites showing consistency with model predictions. (A and B) Strong depletion in Lu from core to rim is broadly consistent with Rayleigh distillation (Fig. 1). Upturn in Lu at garnet rims indicates retrograde dissolution and back-diffusion of Lu. Arrow shows where approximately 50% of Lu is enclosed within core. Hf not plotted for analyses with high Zr (zircon contamination). (C and D) Arcuate distribution of isotopic data on isochron diagrams is consistent with garnet growth (or multiple garnet generations) over timescales exceeding a few hundred kyr (Fig. 6). Difference in oldest vs. youngest garnet separates estimates either the minimum duration of garnet growth, or, for polymetamorphic rocks, the minimum difference in age of different garnet generations. M1 and M3 are regression models 1 and 3 of IsoPlot (McIntyre et al., 1966; York, 1966; Ludwig, 2001). Note the impossibly low initial ϵ_{Hf} (lower than primordial Earth) implied by sample 31a using M3 regression.

of ~ 750 °C can allow partial redistribution of intragranular REE by diffusion, at least in metapelites with likely high $f_{\text{H}_2\text{O}}$. In sample 31a, a distinct break in Y and Lu profiles occurs approximately 1/3 of the way from core to rim (arrows in Fig. 10B), suggesting a hiatus in garnet growth or a major change to mass transport in the matrix (e.g., Chernoff and Carlson, 1999). Considering the occurrence of both Paleozoic and Cenozoic metamorphism in the Himalaya (Gehrels et al., 2003, 2006), the increases in Lu on the right side of the profile, and in both Lu and Y on the left side may well have resulted from resorption associated with polymetamorphism.

3.4. Lu–Hf data

Lu–Hf isochrons for the two Himalayan rocks (Fig. 10C and D; Table 2) exhibit arcuate forms as predicted from theoretical models (Fig. 6). Specifically, the garnet splits with highest and lowest Lu/Hf yield the oldest and youngest apparent ages. For sample 72b, the difference in age is only 700 ± 400 kyr—small, but resolvable by Lu–Hf in this highly radiogenic system—suggesting a single garnet

growth event at ~ 34 Ma. The arcuate form of the isochron in sample 31a is far more pronounced than in 72b, and the MSWD far higher than modeled (>800 vs. <200). A model 3 regression yields an ϵ_{Hf} for sample 31a of ca. -300 , well below primordial Earth, and is not quantitatively meaningful for any Earth process. A model 1 regression yields a higher and more realistic ϵ_{Hf} (-80 ± 60).

4. DISCUSSION

The following discussion expands upon key points described in Section 3, focusing on model results and their implications. Topics include chronologic resolution and inference of garnet growth rates, sources of high MSWDs on isochron diagrams, and broader implications of the Himalayan data.

4.1. Chronologic resolution of different isotopic systems and rates of garnet growth

The Lu–Hf system in metapelitic rocks inherently exerts the strongest chronologic leverage. Strong fractionation of

Table 2
Lu–Hf results for Himalayan samples.

Sample	Lu (ppm)	Hf (ppm)	$^{176}\text{Lu}/^{177}\text{Hf}$	2σ abs error	$^{176}\text{Hf}/^{177}\text{Hf}$	2σ abs error
31a G3	8.718	0.0845	14.83261	0.07416	0.358331	0.000028
31a G2	7.920	0.1312	8.62453	0.04312	0.322136	0.000014
31a G1	8.967	0.2028	6.30387	0.03152	0.309256	0.000014
31a WR	0.383	0.0898	0.60577	0.00303	0.283515	0.000019
72b G2	9.005	0.1404	9.11084	0.04555	0.288158	0.000035
72b G3	10.840	0.2049	7.51069	0.03755	0.287090	0.000014
72b G1	4.979	0.1815	3.89322	0.01947	0.284815	0.000014
72b WR	0.827	0.7049	0.16650	0.00083	0.282509	0.000014

Note: G3, G2, and G1 are different garnet splits from the same sample. WR, whole-rock. Errors for Lu/Hf are $\pm 0.5\%$; error for Hf-isotope ratio is the larger of either the measured in-run error or 0.000014.

Lu into garnet in metapelites, plus faster ingrowth of ^{176}Hf drives this behavior, which can be illustrated in several ways. For example, the higher MSWD in metapelite models for Lu–Hf vs. Sm–Nd implies better chronologic resolution. Alternatively, taking parent-reference isotope ratios of ~ 10 for $^{176}\text{Lu}/^{177}\text{Hf}$ in metapelites, and ~ 2 for $^{176}\text{Lu}/^{177}\text{Hf}$ in metabasites, $^{87}\text{Rb}/^{86}\text{Sr}$, and $^{147}\text{Sm}/^{144}\text{Nd}$, analytical errors of ± 0.000015 for Hf isotopes, ± 0.000007 for Sr isotopes and ± 0.000005 for Nd isotopes propagate to chronologic errors of about 80, 400, 250, and 400 kyr, respectively. These calculations do not take into account uncertainties in parent-reference isotope ratios (typically 0.5%) or the purity of mineral separates.

These calculations assume sample sizes are non-limiting, whereas in practice the scale of sampling may strongly affect a chronologist's ability to separate isotopically distinct materials. Sampling for Lu–Hf requires ~ 250 mg of material, which for typical garnet densities corresponds to a cube of garnet 4–5 mm per side. Thus separation of garnet cores vs. rims is rarely feasible for high-precision Lu–Hf analysis. In contrast, Sm–Nd and Rb–Sr can accommodate much smaller sample sizes, as low as a few mg (e.g., Ducea et al., 2003; Harvey and Baxter, in press), reducing spatial resolution to ~ 1 mm, and potentially permitting direct analysis of chronologic zoning for a wider range of garnets and rocks. Decreasing sample sizes generally increase analytical error, however, degrading chronologic resolution. For example, an increased analytical uncertainty of ± 0.000015 reduces chronologic resolution to ± 500 kyr for Rb–Sr and ± 1 –2 Myr for Sm–Nd.

Can the age disparity between Lu–Hf and Sm–Nd systems be used to infer rates of growth of garnet (Lapen et al., 2003)? In principle yes, because high Lu concentrations in garnet cores should produce older Lu–Hf ages compared to Sm–Nd or Rb–Sr ages. Nonetheless, retrograde dissolution plus diffusion can redistribute Lu towards garnet rims, decreasing apparent age differences after ingrowth of ^{176}Hf . Some studies have also indicated non-uniform distributions of Sm and LREE through a garnet (Skora et al., 2006; Corrie and Kohn, 2008), so Sm–Nd ages might not preferentially reflect growth of garnet rims. Moreover, the small age disparity illustrated for garnet separates (ca. 30% of total garnet growth; Fig. 7), implies relatively large and imprecise extrapolations. Better estimates can be derived either by collecting chronologic zoning profiles directly (if garnet crystals are large; Christensen et al., 1989,

1994; Ducea et al., 2003), or by measuring trace element profiles and integrating compositions directly, as was done by Lapen et al. (2003). Relying on assumed endmember fractionations and models such as Fig. 7 is not advised.

4.2. Garnet growth zoning and high MSWDs

Considering that the chronologic resolution of the different isotopic systems is only a few hundred kyr, high MSWDs for isochrons are expected. Assuming garnet growth durations of Myr to tens of Myr, any mineral separation technique that distinguishes different portions of a garnet must yield high MSWDs because age differences for different portions of the garnet far exceed the analytical resolution. If garnet splits are distinguished on the basis of color (e.g., Kohn et al., 1997), density of inclusions, or other physical attributes, cores may be partially separated from rims, leading to age disparities and a high MSWD when regressed together with a matrix composition. Other processes can cause high MSWDs, however, including inheritance, laboratory error, etc. If garnet growth zoning is advocated as the cause, then specific criteria must be met, most importantly that the oldest split is the most radiogenic, and that the data exhibit the arcuate form exhibited in the simple growth models (Fig. 7).

Accessory phases may also contaminate analyses and lead to high MSWDs. This process was already described well for garnet Lu–Hf and Sm–Nd ages (Scherer et al., 2000). In general, their results predict that increasing contamination pulls isotopic compositions below the true-age isochron. In principle, such an effect could lead to increased MSWDs, or even systematic arcuate distributions of data on isochron diagrams (analogous to Fig. 6A), if late-grown garnet is systematically more affected by contamination. A zircon effect should be identifiable from systematic changes in Zr. For example, a ~ 0.1 ppm increase in Hf due to dissolved zircon with 1 wt% Hf would generally contribute a ~ 4 ppm increase in Zr. Identifying contamination by P- or Ti-rich minerals would be more difficult, as concentrations are relatively high for P (hundreds of ppm) and Ti (thousands of ppm) in garnet.

4.3. Diffusional modification of trace element zoning

Qualitatively, Fig. 9 predicts the effects on isochron diagrams of diffusional modification of Lu zoning. But are

temperatures ever realized that allow such a process to occur? Two lines of evidence suggest so. First, experimentally measured diffusion rates of REE in natural garnets (Van Orman et al., 2002; Tirone et al., 2005) imply characteristic diffusion distances of tens to hundreds of μm for durations as short as 1 Myr at $T = 750^\circ\text{C}$. Second, near-rim increases in Lu in the Himalayan garnets likely result from garnet rim dissolution and back-diffusion, and the length scales of these profiles similarly imply diffusive exchange over distances of tens to hundreds of microns. In contrast, because of its higher valence, Hf^{4+} should diffuse more slowly than REE^{3+} (e.g., Cherniak and Watson, 2003, 2007).

Overall, because of its compatibility yet demonstrable intracrystalline mobility, Lu behaves like the major/minor element Mn, and serves as a useful monitor of dissolution reactions and diffusion, albeit with a lower diffusivity (Tirone et al., 2005). In contrast, Hf behaves like the major/minor element Ca, which diffuses much more slowly than Mn (e.g., Spear and Kohn, 1996). The predicted growth zoning and diffusive behavior of Lu vs. Hf in garnet is directly analogous to that of the major elements Mn vs. Ca, which has been modeled extensively (Florence and Spear, 1991).

4.4. Lu–Hf data from Himalayan rocks

Some of the principal predictions of the models are illustrated by the Himalayan data, including depletions of Lu from core to rim (except at the rim), arcuate isochrons, and high MSWDs, especially for sample 31a. This correspondence supports the use of simple Rayleigh models for understanding and interpreting garnet chronologic data, at least in the context of complementary trace element data (Lapen et al., 2003). The ~ 34 Ma age for sample 72b is consistent with relatively early Himalayan metamorphism of the Greater Himalayan Sequence, and corresponds with an early, presumed prograde, generation of monazite (Kohn et al., 2004, 2005). The extraordinary MSWD in 31a (>800) compared to theoretical models (<200) is understandable in terms of either more protracted growth of garnet than modeled (>40 Myr as indicated by the maximum and minimum ages from 2-point isochrons vs. 10 Myr in the models), or polymetamorphism in which the high Lu/Hf split contains a greater proportion of inherited core, whatever its age, than the lower Lu/Hf splits. The fact that the apparent Lu–Hf ages exceed typical Himalayan ages, and monazite ages from the same rock (Kohn et al., 2004, 2005) by over 200 Myr is consistent with the latter interpretation, in which Paleozoic metamorphism of Greater Himalayan rocks was overprinted by metamorphism associated with the Indo-Asian collision (Gehrels et al., 2003, 2006).

5. CONCLUSIONS

Advances in mass spectrometry have led to some seemingly perplexing results for garnet geochronology, including high MSWDs. These results can be understood in the context of expected growth durations of garnet crystals (Myr to tens of Myr) compared to the chronologic resolution of different isotopic systems (typically several hundred kyr for Lu–Hf, Rb–Sr, and Sm–Nd for bulk separates, and ≤ 1 –2 Myr for

Sm–Nd and Rb–Sr zoning studies. The current models build on previous work by Lapen et al. (2003) and Skora et al. (2006) and provide roadmaps for interpreting isochron diagrams in the context of trace element zoning in garnet crystals, which reflects various processes including prograde garnet growth, kinetically limited mass transport in the rock matrix, and post-growth diffusional modification of zoning (e.g., see Kohn, 2003). Most importantly, interpretation that garnet growth zoning causes high MSWDs implies distinctive arcuate distributions of isotopic data on isochron diagrams.

Durations of garnet growth may possibly be inferred from different chronologic systems (e.g., Lu–Hf vs. Sm–Nd; Lapen et al., 2003), or from data distributions on isochron diagrams (this study). However both approaches implicitly assume systematic trace element zoning in garnet crystals, which must be confirmed before durations can be fully quantified. As pioneered by Christensen et al. (1989), chronologic zoning studies remain the least presumptive means of determining the duration of garnet growth. Advances in microanalysis, rather than bulk garnet separates or combination of different isotopic systems, harbor the greatest potential for improving our understanding of garnet chronology and growth durations.

ACKNOWLEDGMENTS

This material is based upon work supported by the National Science Foundation under Grant Numbers EAR0439733 and EAR0509833, and by Boise State University. Special thanks are due Jeff Vervoort for posing the stimulating conundrum that Lu–Hf garnet ages can have high MSWDs, now understood in the context of this study to result in some cases from protracted growth of garnet over millions of years. Ethan Baxter and Erik Scherer provided incisive reviews that especially helped disabuse the author of some analytical misconceptions, and Daniele Cherniak described preliminary diffusion results for REE and Hf in garnet. Stacey Corrie, Robert King, and Charles Knaack are thanked for their help in deciphering partition coefficients and with trace element and Lu–Hf analysis.

APPENDIX A. SUPPLEMENTARY DATA

Supplementary data associated with this article can be found, in the online version, at [doi:10.1016/j.gca.2008.10.004](https://doi.org/10.1016/j.gca.2008.10.004).

REFERENCES

- Amato J. M., Johnson C. M., Baumgartner L. and Beard B. L. (1999) Rapid exhumation of the Zermatt-Saas ophiolite deduced from high-precision Sm–Nd and Rb–Sr geochronology. *Earth Planet. Sci. Lett.* **171**, 425–438.
- Anzkiewicz R. and Thirlwall M. F. (2003) Improving precision of Sm–Nd garnet dating by H_2SO_4 leaching—a simple solution to phosphate inclusions problem. In *Geochronology: Linking the Isotopic Record with Petrology and Tectonics*, vol. 220 (eds. D. Vance, W. Mueller and I. M. Villa). Geological Society of London, pp. 83–91.
- Anzkiewicz R., Szczepanski J., Mazur S., Storey C., Crowley Q., Villa I. M., Thirlwall M. F. and Jeffries T. E. (2007) Lu–Hf geochronology and trace element distribution in garnet: implications for uplift and exhumation of ultra-high pressure granulites in the Sudetes, SW Poland. *Lithos* **95**, 363–380.

- Baxter E. F. and DePaolo D. J. (2002) Field measurement of high temperature bulk reaction rates: II. Interpretation of results from a field site near Simplon Pass, Switzerland. *Am. J. Sci.* **302**, 465–516.
- Baxter E. F., Ague J. J. and DePaolo D. J. (2002) Prograde temperature-time evolution in the Barrovian type-locality constrained by Sm/Nd garnet ages from Glen Clova, Scotland. *J. Geol. Soc. Lond.* **159**, 71–82.
- Burton K. W., Kohn M. J., Cohen A. S. and O’Nions R. K. (1995) The relative diffusion of Pb, Nd, Sr and O in garnet. *Earth Planet. Sci. Lett.* **133**, 199–211.
- Carlson W. D. (1989) The significance of intergranular diffusion to the mechanism and kinetics of porphyroblast crystallization. *Contrib. Mineral. Petrol.* **103**(1), 1–24.
- Cheng H., King R. L., Nakamura E., Vervoort J. D. and Zhou Z. (2008) Coupled Lu–Hf and Sm–Nd geochronology constrains garnet growth in ultra-high-pressure eclogites from the Dabie orogen. *J. Metamorph. Geol.* **26**, 741–758.
- Cherniak D. J. and Watson E. B. (2003) Diffusion in zircon. *Rev. Mineral. Geochem.* **53**, 113–143.
- Cherniak D. J. and Watson E. B. (2007) Ti diffusion in zircon. *Chem. Geol.* **242**, 470–483.
- Chernoff C. B. and Carlson W. D. (1999) Trace element zoning as a record of chemical disequilibrium during garnet growth. *Geology* **27**(6), 555–558.
- Christensen J. N., Rosenfeld J. L. and DePaolo D. J. (1989) Rates of tectonometamorphic processes from rubidium and strontium isotopes in garnet. *Science* **244**, 1465–1469.
- Christensen J. N., Selverstone J., Rosenfeld J. L. and DePaolo D. J. (1994) Correlation of Rb–Sr geochronology of garnet growth histories from different structural levels within the Tauern Window, Eastern Alps. *Contrib. Mineral. Petrol.* **118**(1), 1–12.
- Connelly J. N. (2006) Improved dissolution and chemical separation methods for Lu–Hf garnet chronometry. *Geochem. Geophys. Geosyst.* **7**. doi:10.1029/2005GC001082.
- Corrie S. L. and Kohn M. J. (2008) Trace element distributions in silicates during prograde metamorphic reactions: implications for monazite formation. *J. Metamorph. Geol.* **26**, 451–464.
- Corrie S. L., Kohn M. J., Vervoort J. D. and Parkinson C. D. (2007) 21 Ma eclogite from the Main Central Thrust sheet, eastern Nepal Himalaya. *EOS—Trans. Am. Geophys. Union* **88**, V41C-0728.
- DeWolf C. P., Zeissler C. J., Halliday A. N., Mezger K. and Essene E. J. (1996) The role of inclusions in U–Pb and Sm–Nd garnet geochronology; stepwise dissolution experiments and trace uranium mapping by fission track analysis. *Geochim. Cosmochim. Acta* **60**, 121–134.
- Ducea M. N., Ganguly J., Rosenberg E. J., Patchett P. J., Cheng W. and Isachsen C. (2003) Sm–Nd dating of spatially controlled domains of garnet single crystals: a new method of high-temperature thermochronology. *Earth Planet. Sci. Lett.* **213**, 31–42.
- Florence F. P. and Spear F. S. (1991) Effects of diffusional modification of garnet growth zoning on P–T path calculations. *Contrib. Mineral. Petrol.* **107**, 487–500.
- Gehrels G. E., DeCelles P. G., Martin A., Ojha T. P., Pinhassi G. and Upreti B. N. (2003) Initiation of the Himalayan orogen as an early Paleozoic thin-skinned thrust belt. *GSA Today* **13**, 4–9.
- Gehrels G. E., DeCelles P. G., Ojha T. P. and Upreti B. N. (2006) Geologic and U–Th–Pb geochronologic evidence for early Paleozoic tectonism in the Kathmandu thrust sheet, central Nepal Himalaya. *Geol. Soc. Am. Bull.* **118**, 185–198.
- Harvey J. and Baxter E. F. (in press) An improved method for TIMS high precision neodymium isotope analysis of very small aliquots (1–10 ng). *Chem. Geol.*, in press.
- Hermann J. (2002) Allanite: thorium and light rare earth element carrier in subducted crust. *Chem. Geol.* **192**, 289–306.
- Hickmott D. D., (1988) Trace element zoning in metamorphic garnets: implications for metamorphic prograde. Doctoral, Massachusetts Institute of Technology.
- Hickmott D. and Spear F. S. (1992) Major- and trace-element zoning in garnets from calcareous pelites in the NW Shelburne Falls Quadrangle, Massachusetts; garnet growth histories in retrograded rocks. *J. Petrol.* **33**(5), 965–1005.
- Hickmott D. D., Shimizu N., Spear F. S. and Selverstone J. (1987) Trace element zoning in a metamorphic garnet. *Geology* **15**, 573–576.
- Hoefs J. (1997) *Stable Isotope Geochemistry*. Springer.
- Hollister L. S. (1966) Garnet zoning: an interpretation based on the Rayleigh fractionation model. *Science* **154**, 1647–1651.
- Hollister L. S. (1969) Contact metamorphism in the Kwoiek Area of British Columbia: an end member of the metamorphic process. *Geol. Soc. Am. Bull.* **80**, 2465–2494.
- Johnston S., Hacker B. R. and Ducea M. N. (2007) Exhumation of ultrahigh-pressure rocks beneath the Hornelen segment of the Nordfjord-Sogn Detachment Zone, western Norway. *Geol. Soc. Am. Bull.* **119**, 1232–1248.
- Jung S. and Mezger K. (2001) Geochronology in migmatites—a Sm–Nd, U–Pb and Rb–Sr study from the Proterozoic Damara belt (Namibia): implications for polyphase development of migmatites in high-grade terranes. *J. Metamorph. Geol.* **19**, 77–97.
- Jung S. and Mezger K. (2003a) Petrology of basement-dominated terranes: I. Regional metamorphic T–t path from U–Pb monazite and Sm–Nd garnet geochronology (Central Damara orogen, Namibia). *Chem. Geol.* **198**, 223–247.
- Jung S. and Mezger K. (2003b) U–Pb garnet chronometry in high-grade rocks—case studies from the central Damara orogen (Namibia) and implications for the interpretation of Sm–Nd garnet ages and the role of high U–Th inclusions. *Contrib. Mineral. Petrol.* **146**, 382–396.
- King R. L., Bebout G. E., Kobayashi K., Nakamura E. and van der Klauw S. N. G. C. (2004) Ultrahigh-pressure metabasaltic garnets as probes into deep subduction zone chemical cycling. *Geochem. Geophys. Geosyst.* **5**, 17.
- King R. L., Vervoort J. D., Kohn M. J., Zirakparvar N. A., Hart G. L., Corrie S. L. and Cheng H. (2007) Promise and pitfalls of Lu/Hf–Sm/Nd garnet geochronology. *EOS—Trans. Am. Geophys. Union* **88**, V31G-02.
- Kohn M. J. (2003) Geochemical zoning in metamorphic minerals. In *Treatise on Geochemistry, vol. 3: The Crust* (ed. R. Rudnick). Elsevier, pp. 229–261.
- Kohn M. J. (2004) Oscillatory- and sector-zoned garnets record cyclic (?) rapid thrusting in central Nepal. *Geochem. Geophys. Geosyst.* **5**, Q12014. doi:10.1029/2004GC000737.
- Kohn M. J. (2008) P–T–t data from central Nepal support critical taper and repudiate large-scale channel flow of the Greater Himalayan Sequence. *Geol. Soc. Am. Bull.* **120**, 259–273.
- Kohn M. J. and Spear F. S. (2000) Retrograde net transfer reaction insurance for pressure–temperature estimates. *Geology* **28**(12), 1127–1130.
- Kohn M. J., Spear F. S. and Valley J. W. (1997) Dehydration-melting and fluid recycling during metamorphism; Rangeley Formation, New Hampshire, USA. *J. Petrol.* **38**(9), 1255–1277.
- Kohn M. J., Wieland M. S., Parkinson C. D. and Upreti B. N. (2004) Miocene faulting at plate tectonic velocity in the Himalaya of central Nepal. *Earth Planet. Sci. Lett.* **228**, 299–310.
- Kohn M. J., Wieland M. S., Parkinson C. D. and Upreti B. N. (2005) Five generations of monazite in Langtang gneisses:

- implications for chronology of the Himalayan metamorphic core. *J. Metamorph. Geol.* **23**, 399–406.
- Kylander-Clark A. R. C., Hacker B. R., Johnson C. M., Beard B. L., Mahlen N. J. and Lapen T. J. (2007) Coupled Lu–Hf and Sm–Nd geochronology constrains prograde and exhumation histories of high- and ultrahigh-pressure eclogites from western Norway. *Chem. Geol.* **242**, 137–154.
- Lagos M., Scherer E. E., Tomaschek F., Munker C., Keiter M., Berndt J. and Ballhaus C. (2007) High precision Lu–Hf geochronology of Eocene eclogite-facies rocks from Syros, Cyclades, Greece. *Chem. Geol.* **243**, 16–35.
- Lapen T. J., Johnson C. M., Baumgartner L. P., Mahlen N. J., Beard B. L. and Amato J. M. (2003) Burial rates during prograde metamorphism of an ultra-high-pressure terrane: an example from Lago di Cignana, western Alps, Italy. *Earth Planet. Sci. Lett.* **215**, 57–72.
- Ludwig K. R. (2001) *IsoPlot/Excel, rev. 2.49, A geochronologic Toolkit for Microsoft Excel*. Berkeley Geochronology Center.
- McIntyre G. A., Brooks C., Compston W. and Turek A. (1966) The statistical assessment of Rb–Sr isochrons. *J. Geophys. Res.* **71**, 5459–5468.
- Münker C., Weyer S., Scherer E. and Mezger K. (2001) Separation of high field strength elements (Nb, Ta, Zr, Hf) and Lu from rock samples for MC-ICPMS measurements. *Geochem. Geophys. Geosyst.* **2**, 2001GC000183.
- Rayleigh J. W. S. (1896) Theoretical considerations respecting the separation of gases by diffusion and similar processes. *Philos. Mag.* **42**, 493.
- Scherer E. E., Cameron K. L. and Blichert-Toft J. (2000) Lu–Hf geochronology: closure temperature relative to the Sm–Nd system and the effects of trace mineral inclusions. *Geochim. Cosmochim. Acta* **64**, 3413–3432.
- Schmidt A., Weyer S., Mezger K., Scherer E. E., Xiao Y., Hoefs J. and Brey G. P. (2008) Rapid eclogitisation of the Dabie-Sulu UHP terrane: constraints from Lu–Hf garnet geochronology. *Earth Planet. Sci. Lett.* **273**, 203–213.
- Skora S., Baumgartner L. P., Johnson C. M., Mahlen N. J., Pilet S. and Hellebrand E. (2006) Diffusion-limited REE uptake by eclogite garnets and its consequences for Lu–Hf and Sm–Nd geochronology. *Contrib. Mineral. Petrol.* doi:10.1007/s00410-006-0128-x.
- Spear F. S. and Kohn M. J. (1996) Trace element zoning in garnet as a monitor of crustal melting. *Geology* **24**, 1099–1102.
- Spear F. S., Kohn M. J., Florence F. and Menard T. (1990) A model for garnet and plagioclase growth in pelitic schists: implications for thermobarometry and P–T path determinations. *J. Metamorph. Geol.* **8**, 683–696.
- Taylor S. R. and McLennan S. M. (1985) *The Continental Crust—Its Composition and Evolution: An Examination of the Geochemical Record Preserved in Sedimentary Rocks*. Blackwell.
- Thöni M. (2002) Sm–Nd isotope systematics in garnet from different lithologies (Eastern Alps): age results, and an evaluation of potential problems for garnet Sm–Nd chronometry. *Chem. Geol.* **185**, 255–281.
- Tirone M., Ganguly J., Dohmen R., Langenhorst F., Hervig R. and Becker H.-W. (2005) Rare earth diffusion kinetics in garnet: experimental studies and applications. *Geochim. Cosmochim. Acta* **69**, 2385–2398.
- Van Orman J. A., Grove T. L., Shimizu N. and Layne G. D. (2002) Rare earth element diffusion in a natural pyrope single crystal at 2.8 GPa. *Contrib. Mineral. Petrol.* **142**(4), 416–424.
- Vervoort J. D. and Blichert-Toft J. (1999) Evolution of the depleted mantle: Hf isotope evidence from juvenile rocks through time. *Geochim. Cosmochim. Acta* **63**, 533–556.
- Vervoort J. D., Patchett P. J., Soderlund U. and Baker M. (2004) Isotopic composition of Yb and the determination of Lu concentrations and Lu/Hf ratios by isotope dilution using MC-ICPMS. *Geochem. Geophys. Geosyst.* **5**, 1029/2004GC000721.
- York D. (1966) Least-squares fitting of a straight line. *Can. J. Phys.* **4**, 1079–1086.
- Zhou B. and Hensen B. J. (1995) Inherited Sm/Nd isotope components preserved in monazite inclusions within garnets in leucogenesis from East Antarctica and implications for closure temperature studies. *Chem. Geol.* **121**(1–4), 317–326.

Associate editor: Alan D. Brandon